

WASP-35b, WASP-48b and WASP-51b: Two new planets and an independent discovery of HAT-P-30b.

B.Enoch¹, D.R.Anderson², S.C.C.Barros³, D.J.A.Brown¹, A.Collier Cameron¹, F.Faedi³, M.Gillon⁴, G.Hébrard^{5,6}, T.A.Lister⁷, D.Queloz⁸, A.Santerne⁹, B.Smalley², R.A.Street⁷, A.H.M.J.Triaud⁸, R.G.West¹⁰, F.Bouchy^{5,6}, J.Bento¹¹, O.Butters¹⁰, L.Fossati¹², C.A.Haswell¹², C.Hellier², S.Holmes¹², E.Jehen⁴, M.Lendl⁸, P.F.L.Maxted², J.McCormac³, G.R.M.Miller¹, V.Moulds³, C.Moutou⁹, A.J.Norton¹², N.Parley¹, F.Pepe⁸, D.Pollacco³, D.Segransan⁸, E.Simpson³, I.Skillen¹³, A.M.S.Smith², S.Udry⁸ and P.J.Wheatley¹¹

ABSTRACT

We report the detection of WASP-35b, a planet transiting a metal-poor ($[\text{Fe}/\text{H}] = -0.15$) star in the Southern hemisphere, WASP-48b, an inflated planet which may have spun-up its slightly evolved host star of $1.75R_{\odot}$ in the Northern hemisphere, and the independent discovery of HAT-P-30b / WASP-51b, a new planet in the Northern hemisphere. Using WASP, RISE, FTS and TRAPPIST photometry, with CORALIE, SOPHIE and NOT spectroscopy, we determine that WASP-35b has a mass of $0.72 \pm 0.06M_J$ and radius of $1.32 \pm 0.03R_J$, and orbits with a period of 3.16 days, WASP-48b has a mass of $0.98 \pm 0.09M_J$, radius of $1.67 \pm 0.08R_J$ and orbits in 2.14 days, while WASP-51b, with an orbital period of 2.81 days, is found to have a mass of $0.76 \pm 0.05M_J$ and radius of $1.42 \pm 0.04R_J$, agreeing with values of $0.71 \pm 0.03M_J$ and $1.34 \pm 0.07R_J$ reported for HAT-P-30b.

¹SUPA, School of Physics and Astronomy, University of St. Andrews, North Haugh, St Andrews, KY16 9SS.

²Astrophysics Group, Keele University, Staffordshire, ST5 5BG, UK.

³Astrophysics Research Centre, School of Mathematics & Physics, Queen's University Belfast, University Road, Belfast, BT7 1NN, UK.

⁴Institut d'Astrophysique et de Géophysique, Université de Liège, Allée de 6 Août, 17, Bat B5C, Liège 1, Belgium.

⁵Institut d'Astrophysique de Paris, UMR7095 CNRS, Université Pierre & Marie Curie, France.

⁶Observatoire de Haute-Provence, CNRS/OAMP, 04870 St Michel l'Observatoire, France

⁷Las Cumbres Observatory, 6740 Cortona Drive Suite 102, Goleta, CA 93117, USA.

⁸Observatoire astronomique de l'Université de Genève, 51 Chemin des Maillettes, 1290 Sauverny, Switzerland.

⁹Laboratoire d'Astrophysique de Marseille, Université d'Aix-Marseille & CNRS, 38 rue Frédéric Joliot-Curie, 13388 Marseille cedex 13, France

¹⁰Department of Physics and Astronomy, University of Leicester, Leicester, LE1 7RH, UK.

¹¹Department of Physics, University of Warwick, Coventry, CV4 7AL, UK

¹²Department of Physics and Astronomy, The Open University, Milton Keynes, MK7 6AA, UK

¹³Isaac Newton Group of Telescopes, Apartado de Correos 321, E-38700 Santa Cruz de Palma, Spain

Subject headings: Stars: planetary systems

1. Introduction

Around 120 transiting exoplanets have now been discovered¹, having both their radii and masses known, and may be subjected to further investigations into their bulk and atmospheric composition (see e.g. Charbonneau et al. 2002, 2005; Fortney et al. 2007; Haswell 2010; Seager & Deming 2010). They show a diverse range of densities and thus internal compositions. Over 80% of those with masses greater than $0.1M_J$ have radii greater than that of Jupiter, and many have extremely low densities which even coreless models struggle to explain (Fortney et al. 2007; Burrows et al. 2007), for example TrES-4b (Mandushev et al. 2007), WASP-17b (Anderson et al. 2010, 2011) and Kepler-7b (Latham et al. 2010). More transiting exoplanets are vital to constrain the formation and evolution of such planets.

Several possible effects on planetary radii have been discussed in the literature, including inflation due to strong heating by irradiation received from the host star (Guillot et al. 1996; Guillot & Showman 2002), ohmic heating from the coupling of magnetic fields and atmospheric flows (Batygin & Stevenson 2010; Batygin et al. 2011) and tidal heating due to the circularisation of close-in exoplanets (Bodenheimer et al. 2001, 2003; Jackson et al. 2008).

Most of the known transiting exoplanets orbit very close to their host star, which produces strong tidal forces between them. The tidal interactions may result in orbital circularisation, synchronisation and decay (Pont 2009). An apparent relationship between period and eccentricity of non-transiting exoplanets, such that planets very close to their host stars have circular orbits while those farther from the stars show a wide range of eccentricities, seems to provide evidence for the tidal circularisation of planetary orbits (Mazeh 2008). However, it had generally been assumed that the masses of planets are too small to synchronise the stellar rotation with the planetary orbit through tidal forces (Mazeh 2008). Some possible exceptions exist for planets with large masses, for example the τ Boo system with a $4M_J$ planet, for which there is evidence for stellar rotation synchronisation (Fares et al. 2009). Recently, CoRoT-11b has been announced to have a ‘peculiar tidal evolution’ (Gandolfi et al. 2011), where the stellar rotation period of 1.7 days is now shorter than the planetary orbital period of 3 days, due to the strong tidal forces causing orbital decay of the planet from a previously approximately synchronised orbital period. The possibility of perhaps unknown close-in exoplanets affecting the stellar spin rate of their host stars produces uncertainty in the use of the gyrochronological age estimate of a star, based on the normal spin down of a star as it ages.

One motivation of the WASP project is to discover enough transiting exoplanets with a wide range of orbital and compositional parameters to allow analyses that may distinguish between

¹www.exoplanet.eu

different models. Recent WASP discoveries help fill in areas of planetary mass-radius parameter space, for example WASP-39b (Faedi et al. 2011) is the least dense sub-Saturn mass planet known.

Here, we announce WASP-35b, WASP-48b and WASP-51b (\equiv HAT-P-30): the positions and magnitudes of each star are given in Table 1. We set out the photometric and spectroscopic observations obtained for each system, before presenting the resulting stellar and system parameters. WASP-48 appears to be a slightly evolved star with a large radius of $1.75R_{\odot}$ and a very short rotation period of around 7 days for its age, around 8 Gyr. WASP-48b may therefore have spun-up its host star despite a mass of only around $1M_J$, due to the star’s inflated radius, although the system has not yet reached synchronisation of stellar rotation period with planetary orbital period (2.15 days). As the host star continues to evolve, increasing significantly in radius, it may engulf WASP-48b, which is currently orbiting at a distance of around 4 times the stellar radius, unless orbital decay due to tidal interactions, such as may have happened to CoRoT-11b (Gandolfi et al. 2011), push the planet far enough away to survive.

Table 1: Star locations.

Star	RA (J2000)	Dec (J2000)	V mag (NOMAD)
WASP-35	05 04 19.6	−06 13 47	10.95
WASP-48	19 24 39.0	+55 28 23	11.66
WASP-51	08 15 48.0	+05 50 12	10.36

2. Observations

2.1. Photometric Observations

The WASP-North and South observatories are located at La Palma, Canary Islands and SAAO, South Africa respectively, and each consist of eight 11cm telescopes of $7.8^{\circ} \times 7.8^{\circ}$ field of view each, on a single fork mount. The cameras scan repeatedly through eight to ten sets of fields each night, taking 30 second exposures. See Pollacco et al. (2006) for more details on the WASP project and the data reduction procedure, and Collier Cameron et al. (2007) and Pollacco et al. (2008) for an explanation of the candidate selection process.

High precision transit light curves of WASP-35, WASP-48 and WASP-51 were obtained with the RISE instrument mounted in the 2.0m Liverpool Telescope (Steele et al. 2008; Gibson et al. 2008) at the Observatorio del Roque de los Muchachos on La Palma, Canary Islands. The data were reduced with the ULTRACAM pipeline (Dhillon et al. 2007) following the same procedure as Barros (2011). Further high quality photometry of WASP-35 was obtained with the 0.6m TRAnsiting Planets and PlanetesImals Small Telescope (TRAPPIST) at La Silla Observatory, Chile, and with the LCOGT 2.0m Faulkes Telescope South (FTS) at Siding Spring Observatory.

Photometric observations for each of WASP-35, WASP-48 and WASP-51 are detailed in Table 2, and shown in Figures 1 to 3.

Table 2: Photometric Observations

Instrument	Date(s)	Num datapoints	
WASP-35			
WASP-N (2 cams)	10/2008-01/2009 10/2009-01/2010	16,748	
WASP-S (1 cam)	10/2009-01/2010		
RISE (V+R)	30/11/2010	630	
TRAPPIST (I+z)	23/12/2010	742	
FTS (z)	01/01/2011	205	
TRAPPIST (I+z)	11/01/2011	300	
WASP-48			
WASP-N (3 cams)	05/2007-07/2007 05/2008-08/2008 05/2009-06/2009 05/2010-09/2010	56,036	
RISE (V+R)	01/07/2010		770
WASP-51			
WASP-N (1 cam)	11/2009-03/2010		4,453
RISE (V+R)	12/01/2011	1,245	

2.2. Spectroscopic Observations

We obtained 3 radial velocity measurements of WASP-35 on the 25 and 26 January 2010 with the Fibre-fed Echelle Spectrograph (FIES) on the 2.5m Nordic Optical Telescope². FIES was used in medium resolution mode (R=46,000) with simultaneous ThAr calibration, and the observations were reduced using the FIEStool package³, then cross-correlated with a high signal-to-noise spectrum of the Sun to obtain the radial velocities. A further nine datapoints were obtained

²operated on the island of La Palma jointly by Denmark, Finland, Iceland, Norway and Sweden, in the Spanish Observatorio del Roque de los Muchachos of the Instituto de Astrofísica de Canarias

³<http://www.not.iac.es/instruments/fies/fiestool/FIEStool.html>

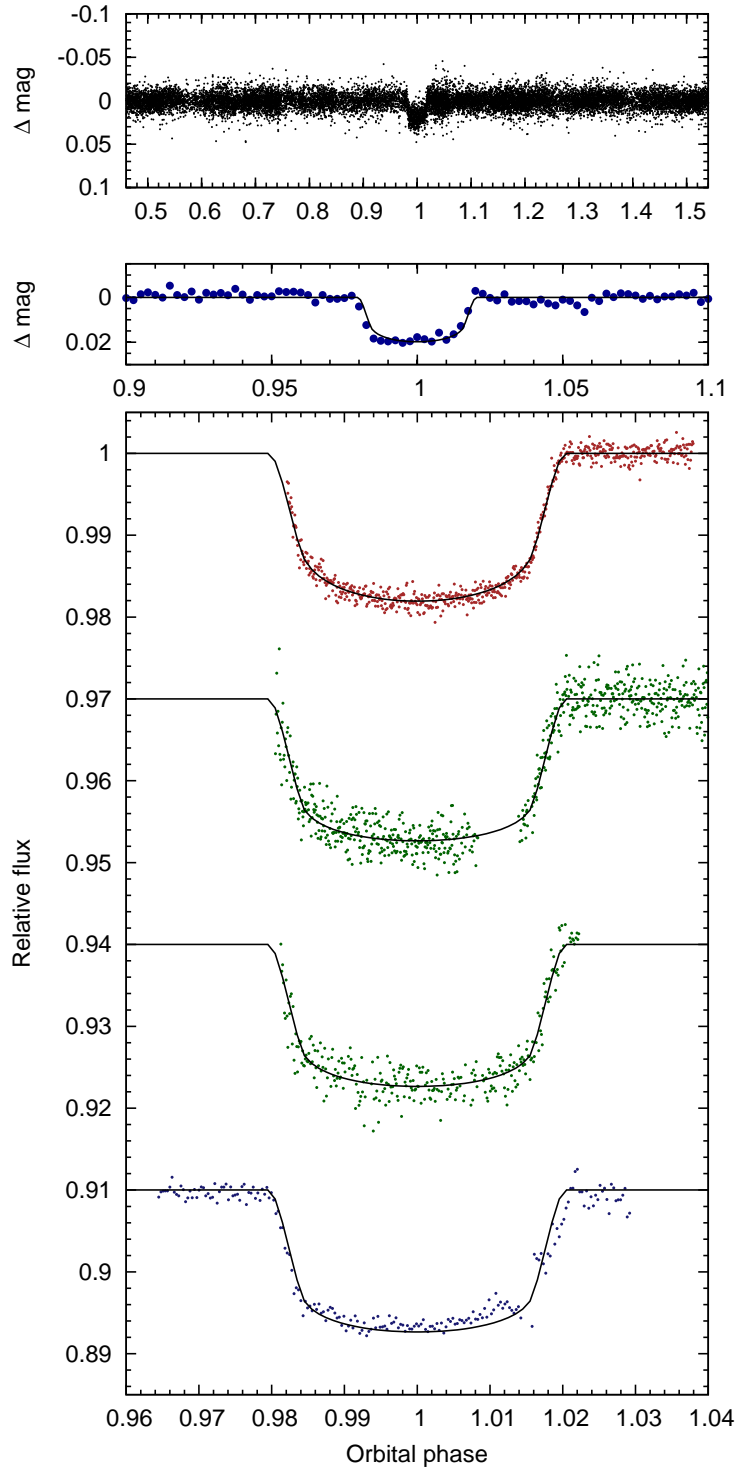


Fig. 1.— Upper plot: WASP-35 discovery lightcurve folded on the orbital period of $P = 3.16$ d. Middle plot: WASP data binned in phase, with bin-width = 11 minutes. Lower plot (top to bottom): transit obtained with the RISE instrument on 30 November 2010, TRAPPIST on 23 December 2010 and 11 January 2011, and FTS on 1 January 2011, lightcurves offset for clarity.

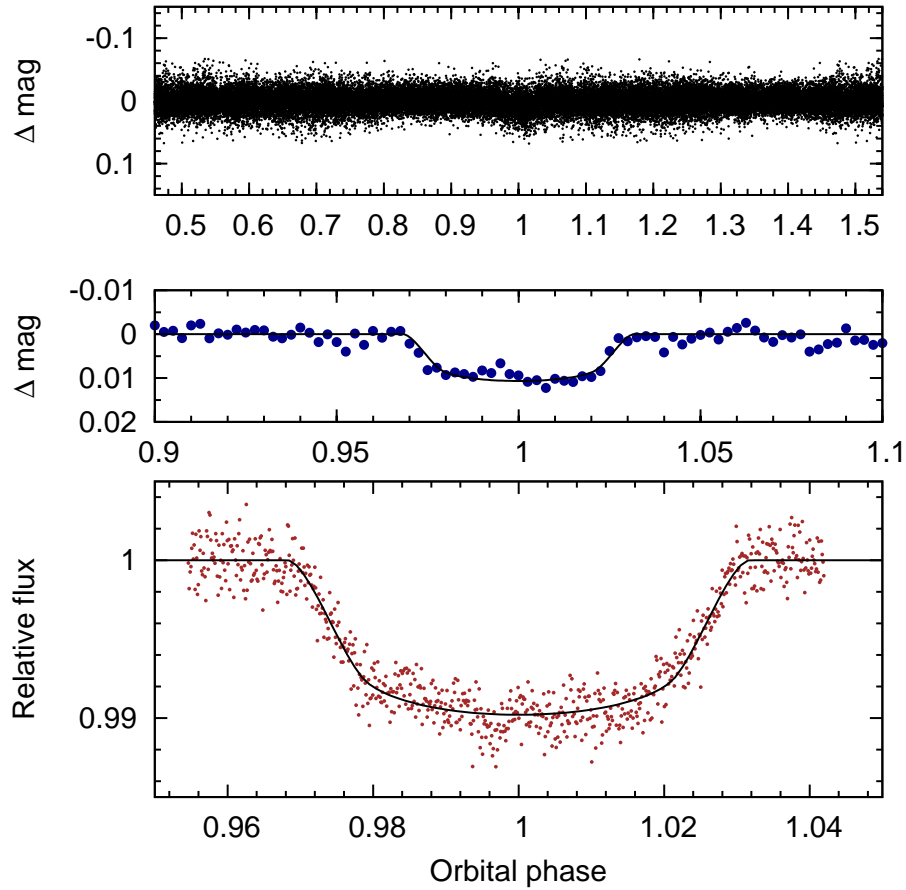


Fig. 2.— Upper plot: WASP-48 discovery lightcurve folded on the orbital period of $P = 2.14$ d. Middle plot: WASP data binned in phase, with bin-width = 8 minutes. Lower plot: transit obtained with the RISE instrument on 1 July 2010.

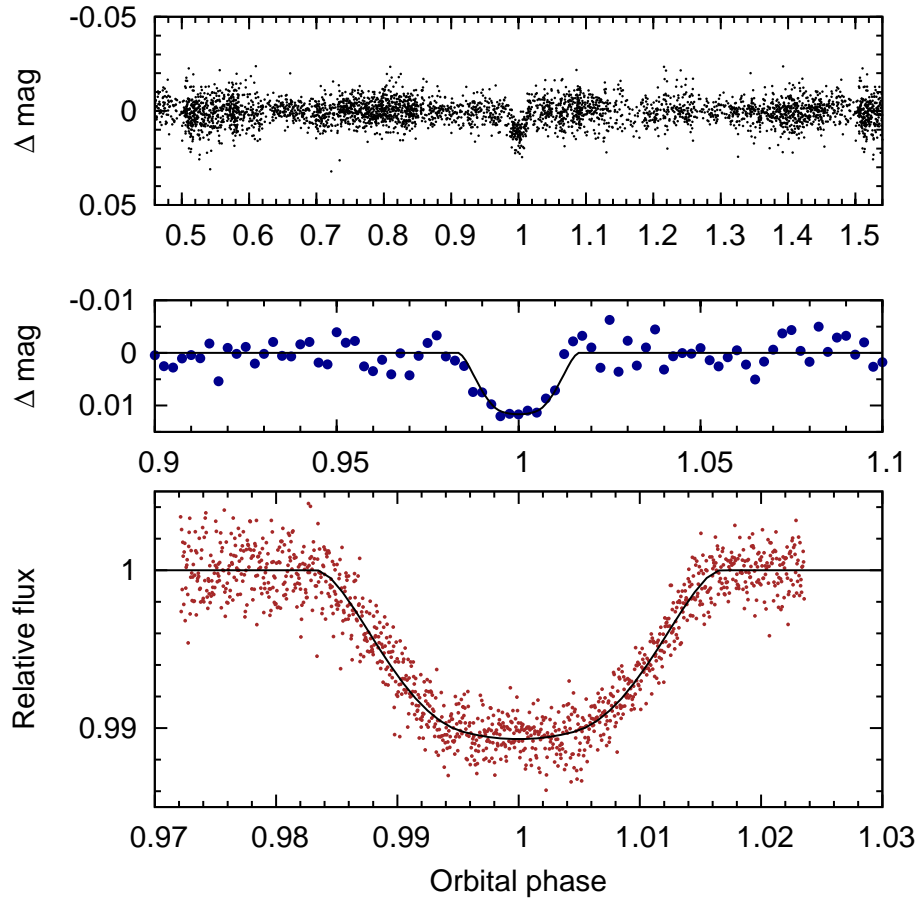


Fig. 3.— Upper plot: WASP-51 discovery lightcurve folded on the orbital period of $P = 2.81$ d. Middle plot: WASP data binned in phase, with bin-width = 10 minutes. Lower plot: transit obtained with the RISE instrument on 12 January 2011.

with the CORALIE echelle spectrograph mounted on the Swiss telescope at the ESO La Silla Observatory in Chile on 5 January 2010 and between 6 and 14 February 2010 and the resulting spectra were processed with the standard data reduction CORALIE pipeline (Baranne et al. 1996; Mayor et al. 2009), plus a correction for the blaze function (Triaud 2010).

WASP-48 was observed spectroscopically with the SOPHIE fibre-fed echelle spectrograph mounted on the 1.93m telescope at Observatoire de Haute-Provence (OHP) (Perruchot et al. 2008; Bouchy et al. 2009). Fourteen datapoints were taken in High Efficiency mode ($R = 40,000$) between 19 April and 18 October 2010, obtaining a signal-to-noise ratio of around 35 for each. Wavelength calibration with a Thorium-Argon lamp was performed to allow the interpolation of the spectral drift of SOPHIE.

Radial velocity observations of WASP-51 were made with the CORALIE and SOPHIE spectrographs. Nine datapoints were taken with SOPHIE between 16 October and 25 November 2010, using the high resolution mode ($R = 75,000$) and obtaining a signal-to-noise ratio of around 20 for each measurement. Ten further datapoints were obtained with CORALIE between 7 December 2010 and 4 January 2011.

The CORALIE guiding camera revealed a faint star located at about $1.5''$ from WASP-51 which was observed simultaneously with WASP-51 through the $3''$ fiber of the SOPHIE spectrograph. Thus, we performed radial velocity blend simulations (Santerne et al, in preparation) in order to investigate whether small bisector variations seen in SOPHIE data are due to this secondary blending star, though the bisector spans are compatible with no variation within the 2σ level. This simulation consisted of producing SOPHIE cross-correlation functions (CCFs) for WASP-51 with the unblended orbital solution seen by CORALIE and blending a single solar star with different systemic radial velocity, distance from WASP-51 and $v \sin i$. With 10,000 Monte Carlo simulations in the ranges 34.6 - 54.6 km s^{-1} for the systemic RV, 1-5 times the distance of WASP-51 and 4 - 40 km s^{-1} for the $v \sin i$ of the blending star, we didn't find any significant model that reproduces the bisector effect seen in the SOPHIE data. For the case of WASP-51, the effect of the blending star on the bisector is less than a few m.s^{-1} . We concluded that the faint star $1.5''$ away didn't affect the SOPHIE CCF of WASP-51.

The radial velocities measured using these spectra are given in Tables 3, 4 and 5, and shown as a function of orbital phase in Figures 4, 5 and 6, along with radial velocity residuals and bisector span variations. The radial velocity measurements show low-amplitude variations, compatible with the existence of orbiting planets, and are not correlated with the bisector spans (available for CORALIE and SOPHIE data) (Queloz et al. 2001), which rules out stellar blend configurations.

Table 3: Radial velocity measurements of WASP-35

BJD–2 400 000	RV (km s ⁻¹)	σ_{RV} (km s ⁻¹)	BS (km s ⁻¹)	Instrument
5201.7298	17.8174	0.0085	–0.0225	CORALIE
5221.5256	17.7386	0.0096		FIES
5222.3276	17.6211	0.0079		FIES
5222.5131	17.6318	0.0093		FIES
5233.6480	17.8050	0.0133	–0.0020	CORALIE
5235.6597	17.6897	0.0084	–0.0446	CORALIE
5236.5322	17.8342	0.0078	–0.0531	CORALIE
5237.5430	17.7133	0.0081	–0.0172	CORALIE
5238.5912	17.6439	0.0080	0.0069	CORALIE
5239.6245	17.8183	0.0088	–0.0402	CORALIE
5240.5331	17.7754	0.0128	–0.0087	CORALIE
5241.5318	17.6446	0.0075	–0.0201	CORALIE

Table 4: Radial velocity measurements of WASP-48 taken with the SOPHIE spectrograph

BJD–2 400 000	RV (km s ⁻¹)	σ_{RV} (km s ⁻¹)	BS (km s ⁻¹)
5305.6441	–19.711	0.024	–0.029
5323.5842	–19.648	0.021	0.015
5328.5784	–19.831	0.025	–0.083
5409.4890	–19.667	0.026	–0.071
5427.5503	–19.747	0.023	–0.062
5429.4215	–19.809	0.026	–0.044
5431.4254	–19.831	0.033	–0.014
5432.3967	–19.589	0.036	–0.059
5476.2714	–19.745	0.021	–0.002
5477.2679	–19.591	0.026	0.044
5482.2945	–19.594	0.022	–0.029
5484.2801	–19.529	0.020	0.042
5485.2880	–19.823	0.026	–0.027
5488.2831	–19.569	0.036	0.009

Table 5: Radial velocity measurements of WASP-51

BJD–2 400 000	RV (km s ⁻¹)	σ_{RV} (km s ⁻¹)	BS (km s ⁻¹)	Instrument
5485.6249	44.611	0.018	-0.023	SOPHIE
5489.6119	44.783	0.018	-0.017	SOPHIE
5495.6696	44.708	0.015	0.100	SOPHIE
5513.6757	44.596	0.013	-0.013	SOPHIE
5519.6870	44.657	0.014	-0.002	SOPHIE
5522.6691	44.677	0.015	0.038	SOPHIE
5523.7176	44.754	0.023	0.084	SOPHIE
5524.6337	44.593	0.022	-0.055	SOPHIE
5525.6785	44.771	0.021	-0.003	SOPHIE
5527.6506	44.586	0.015	0.048	SOPHIE
5537.8023	44.7111	0.0062	-0.0046	CORALIE
5538.8006	44.5639	0.0061	-0.0118	CORALIE
5542.8449	44.7469	0.0073	0.0240	CORALIE
5544.7669	44.6278	0.0065	0.0087	CORALIE
5545.8487	44.7761	0.0066	0.0016	CORALIE
5547.8576	44.6832	0.0074	-0.0027	CORALIE
5561.8052	44.6526	0.0072	0.0241	CORALIE
5562.8426	44.7309	0.0070	-0.0010	CORALIE
5563.7958	44.5945	0.0083	0.0155	CORALIE
5565.7984	44.7353	0.0070	0.0170	CORALIE

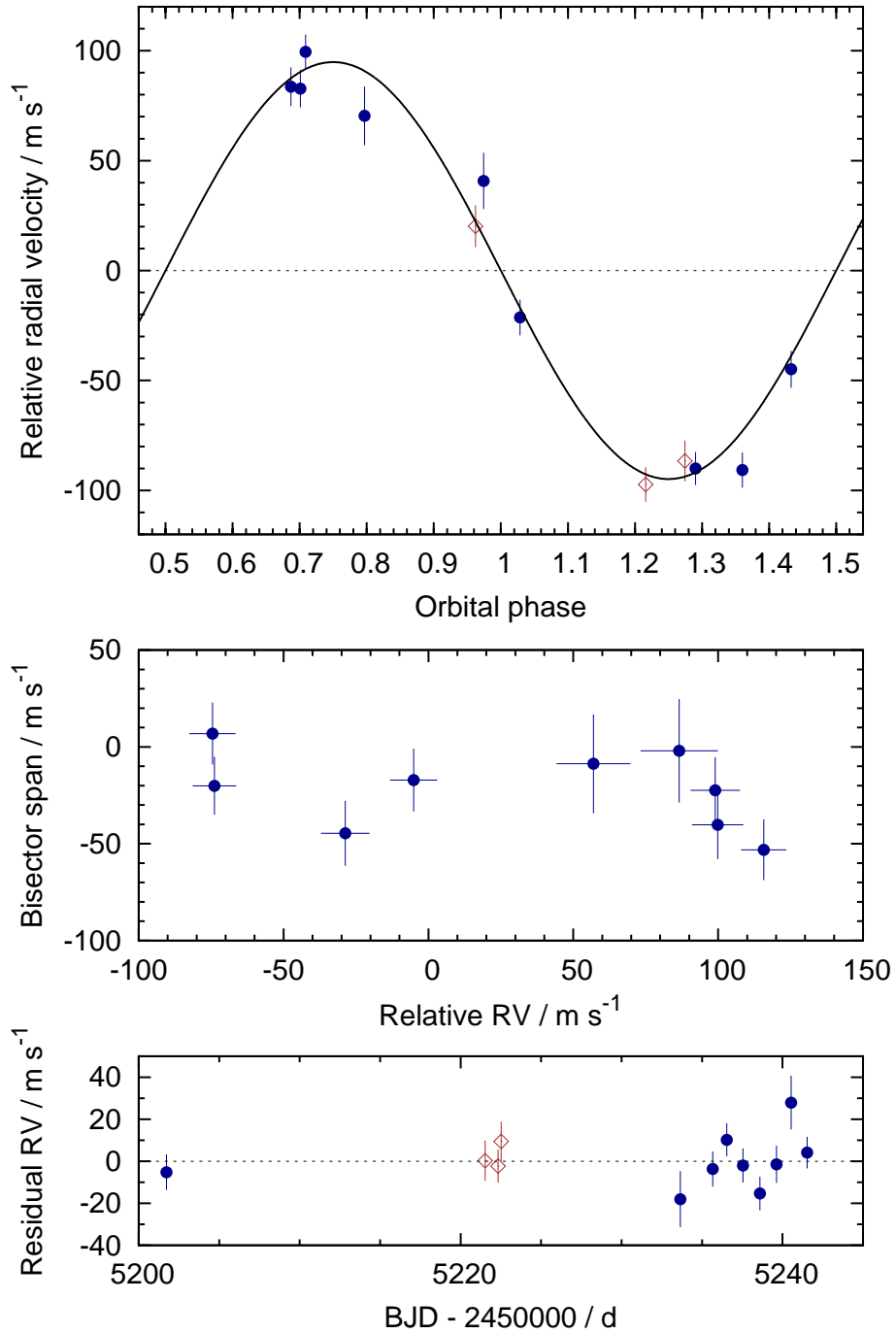


Fig. 4.— Radial velocity measurements for WASP-35: red, open diamonds denote NOT observations, blue circles are from CORALIE. The solid line shown on the top plot is the best-fitting MCMC solution with eccentricity fixed to zero. The centre-of-mass velocity, $\gamma = 17.71 \text{ km s}^{-1}$, was subtracted. The middle plot shows the bisector span variations against radial velocity measurements. The uncertainty in the bisector span measurements are taken to be twice the uncertainty in the radial velocity measurements. The lower plot shows the radial velocity residuals against time.

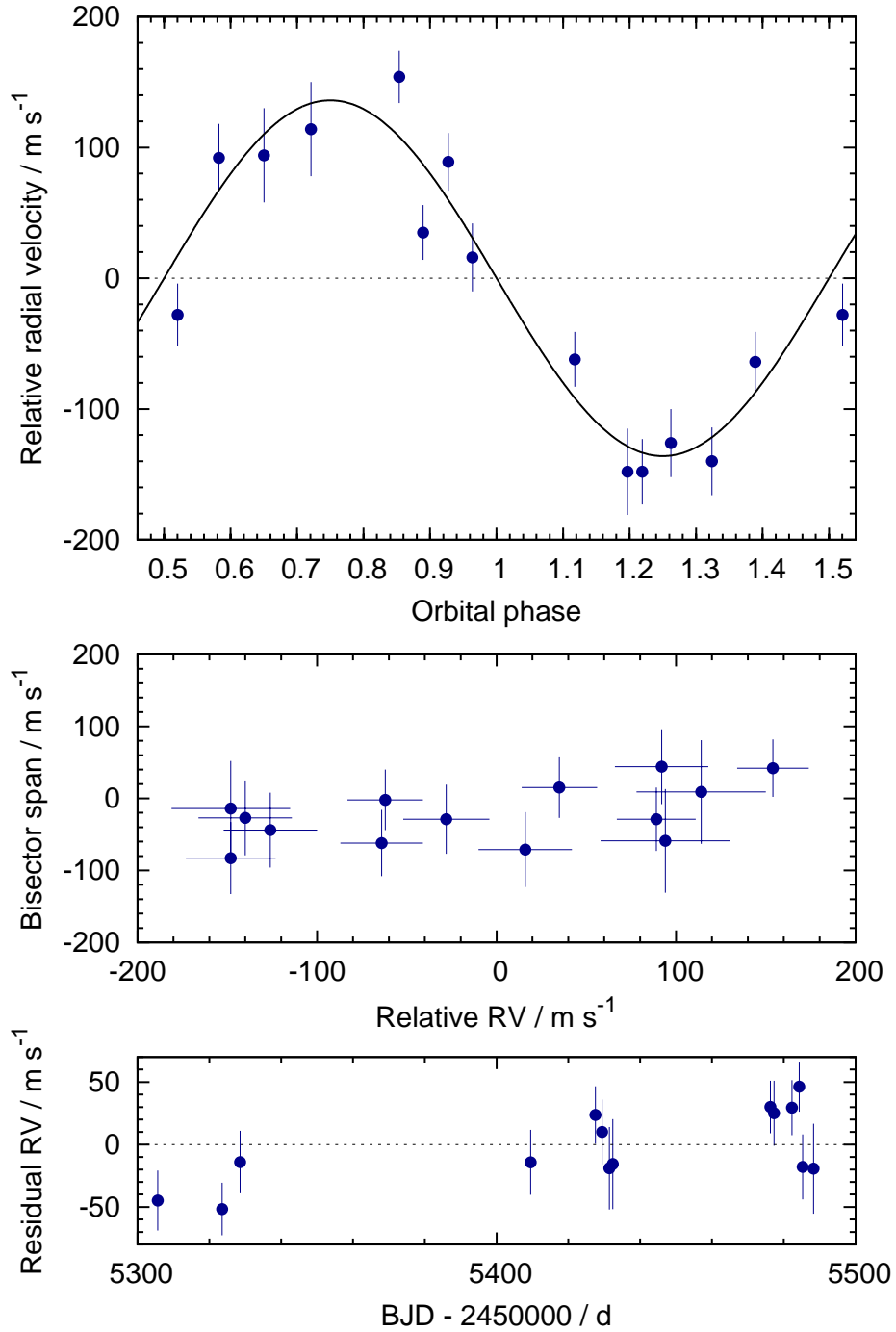


Fig. 5.— Radial velocity measurements for WASP-48: details are as for WASP-35, with centre-of-mass velocity, $\gamma = -19.68 \text{ km s}^{-1}$ here.

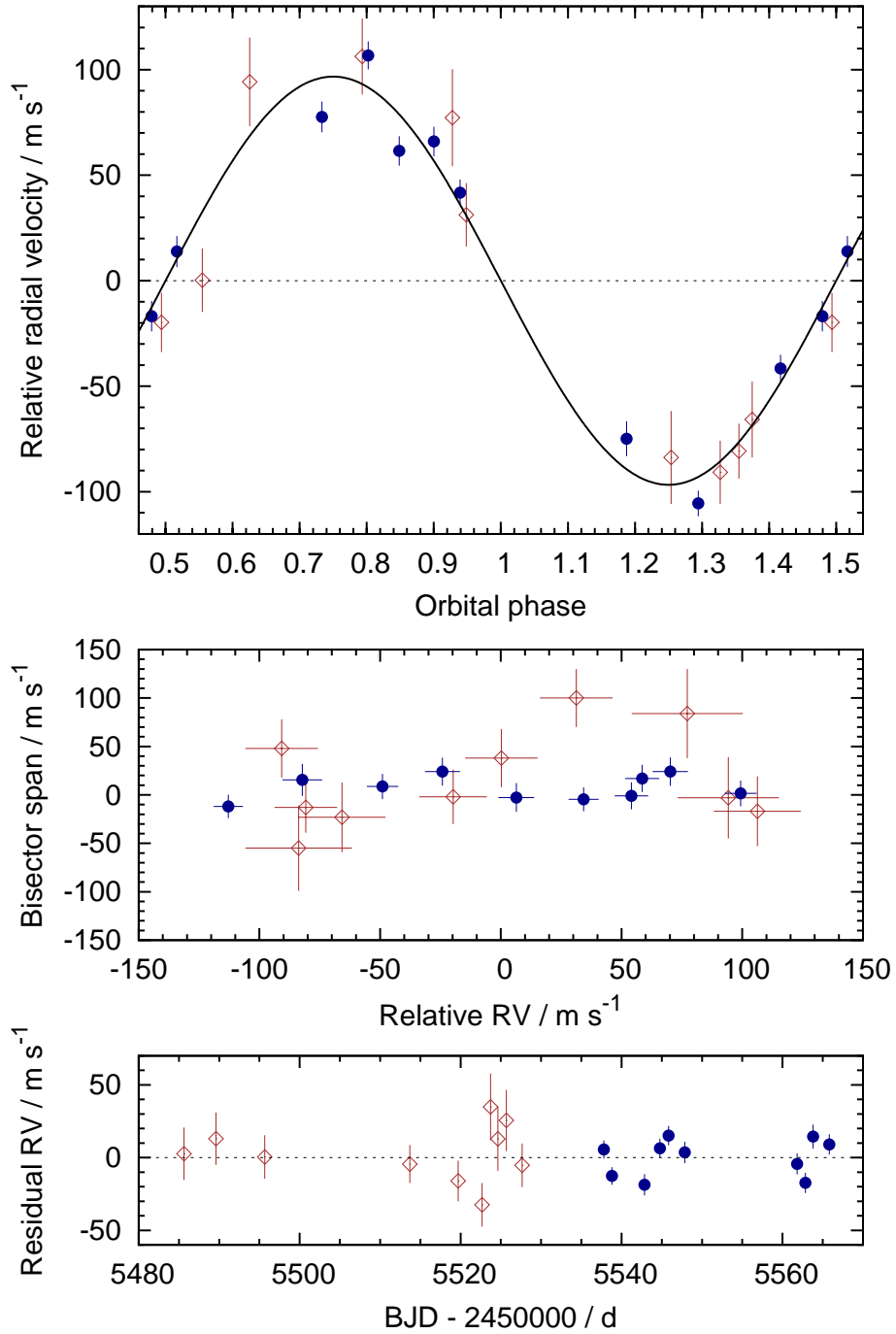


Fig. 6.— Radial velocity measurements for WASP-51: red diamonds and blue circles denote OHP and CORALIE observations, respectively. Details are as for WASP-35, with centre-of-mass velocity, $\gamma = 44.68 \text{ km s}^{-1}$ here.

3. Results and Discussion

3.1. Stellar Parameters

The individual NOT/FIES spectra of WASP-35 were co-added to produce a single spectrum with an average S/N of around 100:1. For WASP-48, the SOPHIE spectra were co-added to produce a spectrum with typical S/N of around 80:1. For WASP-51, the CORALIE spectra were co-added to produce a single spectrum with an average S/N of around 150:1. The standard pipeline reduction products were used in the analysis.

The analysis was performed using the methods given in Gillon et al. (2009). The $H\alpha$ line was used to determine the effective temperature, T_{eff} , while the Na I D and Mg I b lines were used as surface gravity, $\log g$ diagnostics. The elemental abundances were determined from equivalent width measurements of several clean and unblended lines. Atomic line data was mainly taken from the Kurucz & Bell (1995) compilation, but with updated van der Waals broadening coefficients for lines in Barklem et al. (2000) and $\log gf$ values from Gonzalez & Laws (2000), Gonzalez et al. (2001) or Santos et al. (2004). A value for microturbulence, ξ_t , was determined from Fe I using the method of Magain (1984). The parameters obtained from the analyses are listed in Table 6. The quoted error estimates include that given by the uncertainties in T_{eff} , $\log g$ and ξ_t , as well as the scatter due to measurement and atomic data uncertainties.

The projected stellar rotation velocity ($v \sin i$) was determined by fitting the profiles of several unblended Fe I lines. Values for macroturbulence, v_{mac} , of $3.3 \pm 0.3 \text{ km s}^{-1}$, $3.2 \pm 0.3 \text{ km s}^{-1}$ and $4.0 \pm 0.3 \text{ km s}^{-1}$ were assumed for WASP-35, WASP-48 and WASP-51, respectively, based on the calibration by Bruntt et al. (2010), and instrumental FWHM of $0.13 \pm 0.01 \text{ \AA}$, $0.15 \pm 0.01 \text{ \AA}$ and $0.11 \pm 0.01 \text{ \AA}$, respectively, determined from the telluric lines around 6300 \AA . Best fitting values of $v \sin i = 3.9 \pm 0.4 \text{ km s}^{-1}$, $12.2 \pm 0.7 \text{ km s}^{-1}$ and $3.6 \pm 0.4 \text{ km s}^{-1}$, respectively, were obtained.

WASP-51b has been recently announced as HAT-P-30b (Johnson et al. 2011). A discrepancy between their results and ours is the value of host star metallicity: we find a value of $[\text{Fe}/\text{H}] = -0.08 \pm 0.08$ whereas Johnson et al. (2011) report $[\text{Fe}/\text{H}] = 0.13 \pm 0.08$, from an analysis using SME (Spectroscopy Made Easy, Valenti & Piskunov (1996)). The difference is partly due to a different solar metallicity value adopted in the spectral analysis, where we use $\log A(\text{Fe}) = 7.54 \pm 0.03$ from Biemont et al. (1991), which is 0.04 dex higher than the current Asplund et al. (2009) solar value of $\log A(\text{Fe}) = 7.50 \pm 0.04$. We continue to use the Biemont et al. (1991) value for consistency between analyses rather than adjusting to new values as they are announced. Additionally, we allow the microturbulence value to float and be fitted, finding a best-fit value of 1.3 km s^{-1} , in excellent agreement with the calibration in Bruntt et al. (2010), compared to the assumed value of 0.85 km s^{-1} adopted by Valenti & Fischer (2005) and used in Johnson et al. (2011). Using the lower value of microturbulence would increase our $[\text{Fe}/\text{H}]$ abundance by 0.07. The slight differences in T_{eff} and $\log g$ values, where Johnson et al. (2011) find $T_{\text{eff}} = 6300 \pm 90$ and $\log g = 4.36 \pm 0.03$, result in a difference of a further 0.03 dex. These three factors combine to reduce the discrepancy

to only 0.07 dex, which is within the quoted uncertainties.

Table 6: Stellar parameters of WASP-35, WASP-48 and WASP-51 from Spectroscopic Analysis.

Parameter	WASP-35	WASP-48	WASP-51
T_{eff}	6050 ± 100 K	6000 ± 150 K	6250 ± 100 K
$\log g$	4.4 ± 0.1	4.5 ± 0.15	4.3 ± 0.1
ξ_t	1.3 ± 0.1 km s ⁻¹	1.3 ± 0.2 km s ⁻¹	1.3 ± 0.1 km s ⁻¹
$v \sin i$	2.4 ± 0.6 km s ⁻¹	12.2 ± 0.7 km s ⁻¹	3.6 ± 0.4 km s ⁻¹
[Fe/H]	-0.15 ± 0.09	-0.12 ± 0.12	-0.08 ± 0.08
[Na/H]	-0.16 ± 0.11	-0.14 ± 0.07	-0.11 ± 0.05
[Mg/H]	-0.01 ± 0.11	-0.09 ± 0.07	-0.08 ± 0.08
[Al/H]	-	0.02 ± 0.14	-
[Si/H]	-0.06 ± 0.05	0.04 ± 0.08	-0.01 ± 0.09
[Ca/H]	-0.01 ± 0.12	-0.10 ± 0.11	0.05 ± 0.12
[Sc/H]	-0.02 ± 0.07	0.13 ± 0.09	0.01 ± 0.06
[Ti/H]	-0.03 ± 0.10	0.02 ± 0.13	-0.03 ± 0.08
[V/H]	-0.13 ± 0.06	-0.17 ± 0.16	-0.10 ± 0.09
[Cr/H]	-0.10 ± 0.09	0.09 ± 0.16	-0.01 ± 0.06
[Mn/H]	-0.29 ± 0.08	-	-0.27 ± 0.11
[Co/H]	-0.22 ± 0.10	-	-
[Ni/H]	-0.16 ± 0.07	-0.18 ± 0.09	-0.10 ± 0.06
$\log A(\text{Li})$	2.35 ± 0.08	< 1.3	2.96 ± 0.08
Mass	1.10 ± 0.08	$1.09 \pm 0.08 M_{\odot}$	$1.20 \pm 0.09 M_{\odot}$
Radius	1.09 ± 0.14	$1.09 \pm 0.14 R_{\odot}$	$1.28 \pm 0.17 R_{\odot}$

Note: Mass and radius estimates using the Torres et al. (2010) calibration.

The lithium abundance in WASP-35 implies an age of $\gtrsim 2$ Gyr according to the calibration of Sestito & Randich (2005) while the measured $v \sin i$ gives a rotational period of $P_{\text{rot}} \simeq 23 \pm 6.5$ days, assuming $i = 90^\circ$, which yields gyrochronological age of $\sim 6_{-4}^{+5}$ Gyr using the relation of Barnes (2007). A lack of stellar activity is indicated by the absence of Ca II H+K emission in the spectra.

The non-detection of lithium in the WASP-48 spectrum suggests that the star is several Gyr old, and the lack of any Ca H+K emission is consistent with this. However, the stellar rotation rate of 4.5 ± 0.6 days from the $v \sin i$ measurement, implies an age of only $\sim 0.2_{-0.1}^{+0.2}$ Gyr using the Barnes (2007) gyrochronological relation. This discrepancy is discussed further below.

The presence of strong lithium absorption in the WASP-51 spectrum suggests that the star is $\lesssim 1$ Gyr old. The stellar rotation period of 18.0 ± 3.1 days found from the $v \sin i$ measurement results in an age of $\sim 5.6_{-2.9}^{+7.2}$ Gyr, though this can be regarded as an upper limit, since the stellar

rotation rate may be higher due to the unknown value of stellar inclination (i).

3.2. System Parameters

We simultaneously analysed all photometry and radial velocity data using a Markov-Chain Monte Carlo (MCMC) analysis, as set out in Collier Cameron et al. (2007), modified to calculate the mass of the host star with a calibration on T_{eff} , $\log \rho$ and $[\text{Fe}/\text{H}]$ as described in Enoch et al. (2010). The photometry provides the stellar density while the effective temperature and metallicity of the star are obtained through spectral analysis, given above.

We initially allowed the value of the eccentricity of each planetary orbit to float, which resulted in values of $e = 0.057_{-0.032}^{+0.064}$, $e = 0.058_{-0.035}^{+0.058}$ and $e = 0.040_{-0.028}^{+0.044}$ for WASP-35b, WASP-48b and WASP-51b, respectively. The eccentricity of all three orbits are consistent with zero based on the Lucy-Sweeney test (Lucy & Sweeney 1971) on the data for each system, which yields 100% probability that these eccentricity values could be due to chance if the underlying orbit were circular for all three systems. With no strong evidence for eccentricity in the orbits, we then performed second analyses of all systems, fixing the eccentricities to zero.

The MCMC results for WASP-48b reveal a slightly evolved star with a large radius of $1.75 R_{\odot}$ (discussed below). This radius is around $0.6R_{\odot}$ greater than expected for that of a star of the same mass on the Main Sequence. To explore this, we performed a further analysis, imposing a Main Sequence constraint on WASP-48, such that a Gaussian prior is used on the stellar radius at each step in the analysis, centred on radius $R_* = M_*^{0.8}$, again allowing the eccentricity to float. This forced the stellar radius estimate down to $1.13R_{\odot}$, artificially inflating the eccentricity estimate to 0.38 ± 0.04 to compensate, since the stellar radius is calculated from the photometry, including a term $\frac{1+e\sin\omega}{\sqrt{1-e^2}}$: an eccentricity of 0.4 produces a stellar radius value 0.65 times that of the estimate with eccentricity at zero. However, the Lucy-Sweeney test result is still 100%, and there is no evidence for such a high eccentricity in the radial velocity curve, where the χ^2 values are 33.3 and 8.6 for eccentric and circular orbits, respectively. Imposing the Main Sequence constraint with the eccentricity held fixed at zero decreases the stellar radius to $1.31 \pm 0.09R_{\odot}$ and decreases the impact parameter from 0.7 to 0.4 to compensate: such a reduction in impact parameter leads directly to a stellar radius estimate 0.70 times smaller. However, the much lower impact parameter estimate produces a model that does not well match the high quality follow up photometric data: compare the fit to ingress and egress in Figure 7, showing the lower impact parameter model, with that in Figure 2. Since neither analysis with Main Sequence constraint imposed produces realistic models for the photometry and spectroscopy, the results from the analysis with no Main Sequence constraint are clearly preferred.

We also tested the imposition of the Main Sequence constraint on WASP-35 and WASP-51, producing negligible change in all parameters, well within the parameter uncertainties, which implies that the photometry is sufficient to well constrain the results.

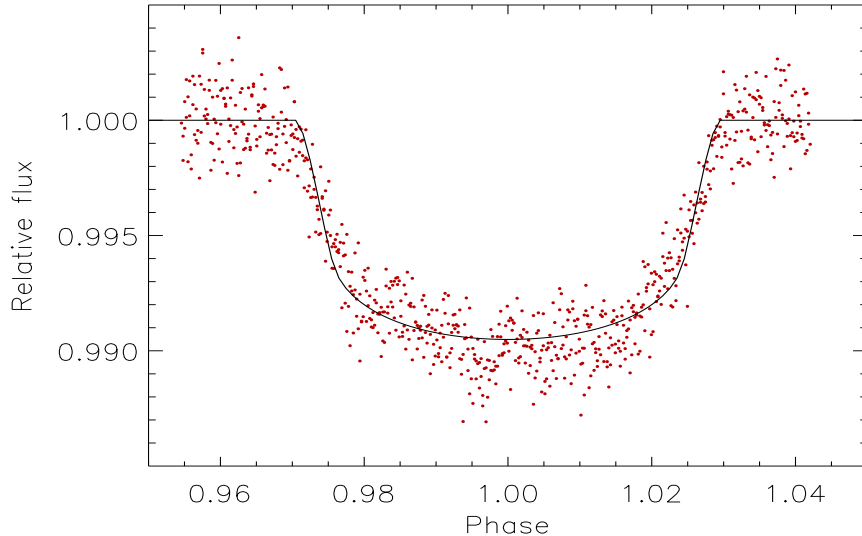


Fig. 7.— RISE photometry shown with the low impact parameter ($b=0.4$) model; a poor fit compared to the fit with $b=0.7$ in Figure 2.

The best-fit parameters for each systems, with eccentricity fixed to zero and no Main Sequence constraint imposed, are given in Table 7. WASP-35 is found to have a mass of $1.07 \pm 0.02 M_{\odot}$ and radius of $1.09 \pm 0.02 R_{\odot}$, while WASP-35b has a mass of $0.72 \pm 0.06 M_J$ and radius of $1.32 \pm 0.03 R_J$, giving a density of $0.32 \pm 0.03 \rho_J$. For WASP-48, the best-fit model gives a stellar mass of $1.19 \pm 0.04 M_{\odot}$ and radius of $1.75 \pm 0.07 R_{\odot}$, giving a stellar density of $0.22 \pm 0.02 \rho_{\odot}$. WASP-48b is found to have a mass of $0.98 \pm 0.09 M_J$ and radius of $1.67 \pm 0.08 R_J$, giving a density of $0.21^{+0.04}_{-0.03} \rho_J$.

The best-fit result for WASP-51 gave a stellar mass $1.18 \pm 0.03 M_{\odot}$, stellar radius $1.33 \pm 0.03 R_{\odot}$, planetary mass $0.76 \pm 0.05 M_J$, planetary radius $1.42 \pm 0.04 R_J$, giving a density of $0.26 \pm 0.02 \rho_J$. Under the name HAT-P-30b, based on HAT-5 (Arizona) and HAT-9 (Hawaii) photometry of a total of around 3,200 good datapoints, follow-up high quality photometric observations with Kepler-Cam on the FLWO 1.2m telescope, and Keck and Subaru radial velocity measurements, Johnson et al. (2011) report a planetary mass of $0.71 \pm 0.03 M_J$, and radius of $1.34 \pm 0.07 R_J$, which agree with our values.

3.3. Isochrone Analysis

The values for stellar density, effective temperature and metallicity from the MCMC analyses (MS constraint off, eccentricity fixed to zero) were used in an interpolation of the Padova stellar

Table 7: System Parameters from simultaneous MCMC analysis of all photometric and spectroscopic data.

Parameter	Symbol	WASP-35	WASP-48	WASP-51
Period (days)	P	3.161575 ± 0.000002	2.143634 ± 0.000003	2.810603 ± 0.000008
Transit Epoch (HJD)	T_0	5531.47907 ± 0.00015	5364.55043 ± 0.00027	5571.70057 ± 0.00020
Transit duration (days)	D	0.1278 ± 0.0005	0.1327 ± 0.0013	0.0920 ± 0.0008
Planet/Star area ratio	R_p^2/R_*^2	0.0154 ± 0.0001	0.0096 ± 0.0002	0.0122 ± 0.0002
Impact Parameter	b	0.30 ± 0.04	0.73 ± 0.03	0.87 ± 0.01
Stellar Reflex Velocity (ms^{-1})	K_1	$94.82^{+7.28}_{-6.92}$	$136.02^{+11.07}_{-11.44}$	$96.70^{+6.07}_{-6.04}$
Centre-of-mass Velocity (kms^{-1})	γ	17.72 ± 0.01	-19.683 ± 0.001	44.6768 ± 0.0001
Orbital separation (AU)	a	0.04317 ± 0.00028	0.03444 ± 0.00043	0.04118 ± 0.00031
Orbital inclination (deg)	i	$87.96^{+0.31}_{-0.25}$	$80.09^{+0.69}_{-0.55}$	$82.48^{+0.14}_{-0.17}$
Orbital eccentricity	e	0 (fixed)	0 (fixed)	0 (fixed)
Orbital distance / radius ratio	a/R_*	8.53 ± 0.19	$4.23^{+0.24}_{-0.19}$	6.67 ± 0.17
Stellar mass (M_\odot)	M_*	1.07 ± 0.02	1.19 ± 0.04	1.18 ± 0.03
Stellar radius (R_\odot)	R_*	1.09 ± 0.02	1.75 ± 0.07	1.33 ± 0.03
Stellar surface gravity ($\log g_\odot$)	$\log g_*$	4.40 ± 0.01	4.03 ± 0.03	4.26 ± 0.01
Stellar density (ρ_\odot)	ρ_*	0.83 ± 0.03	0.22 ± 0.02	0.50 ± 0.02
Stellar metallicity	[Fe/H]	-0.15 ± 0.09	-0.12 ± 0.12	-0.08 ± 0.08
Stellar effective temperature	T_{eff}	5990 ± 80	5920 ± 150	6250 ± 100
Planet mass (M_J)	M_p	0.72 ± 0.06	0.98 ± 0.09	0.76 ± 0.05
Planet radius (R_J)	R_p	1.32 ± 0.03	1.67 ± 0.08	1.42 ± 0.04
Planet surface gravity ($\log g_J$)	$\log g_p$	2.98 ± 0.04	4.03 ± 0.03	2.93 ± 0.03
Planet density (ρ_J)	ρ_p	0.32 ± 0.03	0.21 ± 0.04	0.26 ± 0.02
Planet temperature (A=0, F=1) (K)	T_{eq}	1450 ± 20	2030 ± 70	1710 ± 30

evolution tracks (Girardi et al. 2002; Marigo et al. 2008), shown in Figures 8, 9 and 10. This resulted in an age for WASP-35 of 5.01 ± 1.16 Gyr and a mass of $1.03 \pm 0.04M_{\odot}$.

WASP-48 was found to have an age of $7.9_{-1.6}^{+2.0}$ Gyr, and mass of $1.08 \pm 0.06M_{\odot}$, supporting the results from the MCMC analyses and lack of lithium and Ca H+K that WASP-48 is an old, slightly evolved star. However, the inferred age from the stellar rotation period is still only $0.6_{-0.2}^{+0.4}$ Gyr when based on a rotational period of 7.2 ± 0.5 days found from the larger stellar radius of $1.75 \pm 0.07R_{\odot}$ (with $v \sin i \cong 12.2 \pm 0.7 \text{ km s}^{-1}$, as before). This apparent contradiction may be due to stellar spin-up by the planet. The close orbits of most known transiting exoplanets produce strong tidal forces between the planet and host star, which lead eventually to orbital circularisation, synchronisation and decay. There is evidence for tidal circularisation among the known transiting exoplanets, seen in the period-eccentricity relation where planets with very short orbital periods have circular orbits while those with longer periods show a range of eccentricities, but the synchronisation of stellar rotation is generally ruled out for most known planet-star systems, with timescales orders of magnitude larger than the Hubble time (Mazeh 2008; Pont 2009). A few exceptions exist where the companion is massive, e.g. the unique case of τ Boo for which the planetary orbital period coincides closely with the mean rotation period of the stellar differential rotation pattern determined from the Zeeman-Doppler imaging (Fares et al. 2009). WASP-48b orbits with a period of 2.14 days ($a = 0.034$ AU), and while it is not a massive companion, the evolved nature of the star giving a radius of $1.75 R_{\odot}$ results in a relatively short stellar tidal synchronisation time of 11_{-2}^{+3} Gyr. A full tidal analysis will be discussed in the forthcoming paper of Brown (in prep).

For WASP-51, the interpolation yields an age of $4.0_{-0.8}^{+1.0}$ Gyr, and mass of $1.16 \pm 0.04M_{\odot}$.

An alternative analysis was also performed using the Yonsei-Yale isochrones (Demarque et al. 2004), which produced an age estimate of 4_{-1}^{+2} Gyr and a mass estimate of $1.04 \pm 0.04M_{\odot}$ for WASP-35, $6.0_{-1.0}^{+2.0}$ Gyr and $1.14_{-0.07}^{+0.06}M_{\odot}$ for WASP-48 and $3.0_{-0.5}^{+1.0}$ Gyr and $1.20_{-0.05}^{+0.03}M_{\odot}$ for WASP-51.

The results of both isochrone analyses are consistent within uncertainties, though the Padova interpolations yield higher ages for each system than the Yonsei-Yale interpolations, and mass values agree with the calibrated values from the MCMC analysis of $1.08 \pm 0.03M_{\odot}$, $1.19 \pm 0.04M_{\odot}$ and $1.18 \pm 0.02M_{\odot}$ for WASP-35, WASP-48 and WASP-51, respectively.

4. Summary

We have presented observations of WASP-35b, WASP-48b and WASP-51b, new transiting exoplanets of $0.72 M_J$ and $1.32 R_J$, $0.98 M_J$ and $1.67 R_J$, and $0.76 M_J$ and $1.42 R_J$, respectively. We have obtained photometry from both WASP-North and -South instruments, as well as high-quality follow-up photometry from RISE, FTS and TRAPPIST. Radial velocity measurements from the FIES, SOPHIE and CORALIE instruments allowed us to confirm the planetary nature of the companions.

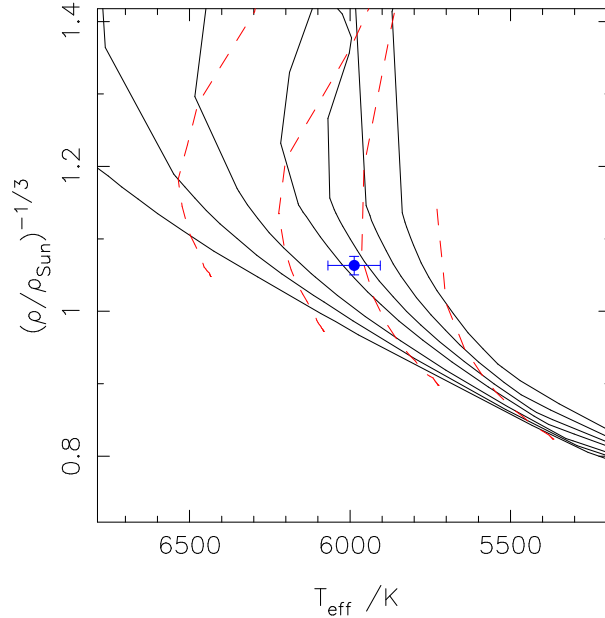


Fig. 8.— Isochrone tracks from Marigo et al. (2008) for WASP-35. Isochrones (solid lines, left to right) are: 1.0, 1.99, 3.16, 5.01, 6.30, 7.94, 10.0 Gyr. Evolutionary tracks (dashed lines) are for 1.2, 1.1, 1.0, 0.9 M_{\odot} stars.

WASP-48b may have spun-up its slightly evolved host star, which shows a high $v \sin i$ value, otherwise contradicting the estimated stellar age of around 8 Gyr. WASP-51b has been recently announced as HAT-P-30b, with mass $0.71M_J$ and radius $1.34R_J$, values that agree with our results, within uncertainties.

WASP-North is hosted by the Isaac Newton Group on La Palma and WASP-South is hosted by the South African Astronomical Observatory (SAAO) and we are grateful for their ongoing support and assistance. Funding for WASP comes from consortium universities and from the UK’s Science and Technology Facilities Council. The RISE instrument mounted on the Liverpool Telescope was designed and built with resources made available from Queen’s University Belfast, Liverpool John Moores University and the University of Manchester. The Liverpool Telescope is operated on the island of La Palma by Liverpool John Moores University in the Spanish Observatorio del Roque de los Muchachos of the Instituto de Astrofísica de Canarias with financial support from the UK Science and Technology Facilities Council. We thank Tom Marsh for the use of the ULTRACAM pipeline. TRAPPIST is a project funded by the Belgian Fund for Scientific Research (FNRS) under the grant FRFC 2.5.594.09.F, with the participation of the Swiss National Science Foundation (SNF). M. Gillon and E. Jehin are FNRS Research Associates. The research leading to these results has received funding from the European Community’s Seventh Framework Programme (FP7/2007-2013) under grant agreement number RG226604 (OPTICON).

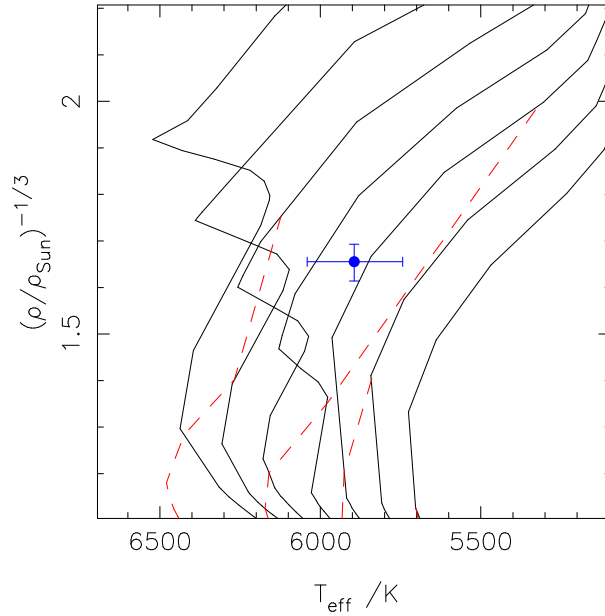


Fig. 9.— Isochrone tracks from Marigo et al. (2008) for the slightly evolved WASP-48 (~ 8 Gyr, $1.75R_{\odot}$). Isochrones (solid lines, left to right) are 3.16, 3.98, 5.01, 6.30, 7.94, 10.0, 12.5 Gyr. Evolutionary tracks (dashed lines) are for 1.2, 1.1, 1.0, 0.9 M_{\odot} stars.

REFERENCES

- Anderson, D. R., Hellier, C., Gillon, M., et al. 2010, *ApJ*, 709, 159
- Anderson, D. R., Smith, A. M. S., Lanotte, A. A., et al. 2011, ArXiv e-prints
- Asplund, M., Grevesse, N., Sauval, A. J., & Scott, P. 2009, *ARA&A*, 47, 481
- Baranne, A., Queloz, D., Mayor, M., et al. 1996, *A&ASupp*, 119, 373
- Barklem, P. S., Piskunov, N., & O’Mara, B. J. 2000, *A&AS*, 142, 467
- Barnes, S. A. 2007, *ApJ*, 669, 1167
- Barros, S. 2011, in prep
- Batygin, K. & Stevenson, D. J. 2010, *ApJ*, 714, L238
- Batygin, K., Stevenson, D. J., & Bodenheimer, P. H. 2011, ArXiv e-prints
- Biemont, E., Baudoux, M., Kurucz, R. L., Ansbacher, W., & Pinnington, E. H. 1991, *A&A*, 249, 539
- Bodenheimer, P., Laughlin, G., & Lin, D. N. C. 2003, *ApJ*, 592, 555

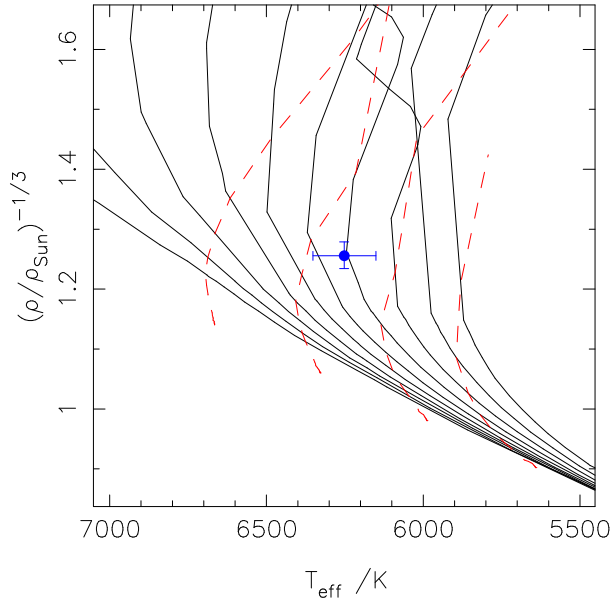


Fig. 10.— Isochrone tracks from Marigo et al. (2008) for WASP-51. Isochrones (solid lines, left to right) are: 1.0, 1.25, 1.58, 1.99, 2.51, 3.16, 3.98, 5.01, 6.30, 7.94 Gyr. Evolutionary tracks (dashed lines) shown are for 1.3, 1.2, 1.1, 1.0 M_{\odot} stars.

Bodenheimer, P., Lin, D. N. C., & Mardling, R. A. 2001, *ApJ*, 548, 466

Bouchy, F., Hébrard, G., Udry, S., et al. 2009, *A&A*, 505, 853

Brown, D. e. a. in prep, in prep

Bruntt, H., Bedding, T. R., Quirion, P. O., et al. 2010, *MNRAS*, 405, 1907

Burrows, A., Hubeny, I., Budaj, J., & Hubbard, W. B. 2007, *ApJ*, 661, 502

Charbonneau, D., Allen, L. E., Megeath, S. T., et al. 2005, *ApJ*, 626, 523

Charbonneau, D., Brown, T. M., Noyes, R. W., & Gilliland, R. L. 2002, *ApJ*, 568, 377

Collier Cameron, A., Wilson, D. M., West, R. G., et al. 2007, *MNRAS*, 380, 1230

Demarque, P., Woo, J., Kim, Y., & Yi, S. K. 2004, *ApJS*, 155, 667

Dhillon, V. S., Marsh, T. R., Stevenson, M. J., et al. 2007, *MNRAS*, 378, 825

Enoch, B., Collier Cameron, A., Parley, N. R., & Hebb, L. 2010, *A&A*, 516, A33+

Faedi, F., Barros, S. C. C., Anderson, D. R., et al. 2011, *ArXiv e-prints*

Fares, R., Donati, J., Moutou, C., et al. 2009, *MNRAS*, 398, 1383

- Fortney, J. J., Marley, M. S., & Barnes, J. W. 2007, *ApJ*, 659, 1661
- Gandolfi, D., Lanza, A. F., & Damiani, C. 2011, *Detection and Dynamics of Transiting Exoplanets*, St. Michel l’Observatoire, France, Edited by F. Bouchy; R. Díaz; C. Moutou; *EPJ Web of Conferences*, Volume 11, id.05006, 11, 5006
- Gibson, N. P., Pollacco, D., Simpson, E. K., et al. 2008, *A&A*, 492, 603
- Gillon, M., Smalley, B., Hebb, L., et al. 2009, *A&A*, 496, 259
- Girardi, L., Bertelli, G., Bressan, A., et al. 2002, *A&A*, 391, 195
- Gonzalez, G. & Laws, C. 2000, *AJ*, 119, 390
- Gonzalez, G., Laws, C., Tyagi, S., & Reddy, B. E. 2001, *AJ*, 121, 432
- Guillot, T., Burrows, A., Hubbard, W. B., Lunine, J. I., & Saumon, D. 1996, *ApJ*, 459, L35+
- Guillot, T. & Showman, A. P. 2002, *A&A*, 385, 156
- Haswell, C. A. 2010, *Transiting Exoplanets* (Cambridge University Press, ISBN: 9780521139380)
- Jackson, B., Greenberg, R., & Barnes, R. 2008, *ApJ*, 681, 1631
- Johnson, J. A., Winn, J. N., Hartman, J. D., et al. 2011, *ArXiv e-prints*
- Kurucz, R. & Bell, B. 1995, *Atomic Line Data* (R.L. Kurucz and B. Bell) Kurucz CD-ROM No. 23. Cambridge, Mass.: Smithsonian Astrophysical Observatory, 1995., 23
- Latham, D. W., Borucki, W. J., Koch, D. G., et al. 2010, *ApJL*, 713, L140
- Lucy, L. B. & Sweeney, M. A. 1971, *AJ*, 76, 544
- Magain, P. 1984, *A&A*, 134, 189
- Mandushev, G., O’Donovan, F. T., Charbonneau, D., et al. 2007, *ApJL*, 667, L195
- Marigo, P., Girardi, L., Bressan, A., et al. 2008, *A&A*, 482, 883
- Mayor, M., Udry, S., Lovis, C., et al. 2009, *A&A*, 493, 639
- Mazeh, T. 2008, in *EAS Publications Series*, Vol. 29, *EAS Publications Series*, ed. M.-J. Goupil & J.-P. Zahn, 1–65
- Perruchot, S., Kohler, D., Bouchy, F., et al. 2008, in *Society of Photo-Optical Instrumentation Engineers (SPIE) Conference Series*, Vol. 7014, *Society of Photo-Optical Instrumentation Engineers (SPIE) Conference Series*
- Pollacco, D., Skillen, I., Collier Cameron, A., et al. 2008, *MNRAS*, 385, 1576

- Pollacco, D. L., Skillen, I., Cameron, A. C., et al. 2006, *PASP*, 118, 1407
- Pont, F. 2009, *MNRAS*, 396, 1789
- Queloz, D., Henry, G. W., Sivan, J. P., et al. 2001, *A&A*, 379, 279
- Santos, N. C., Israelian, G., & Mayor, M. 2004, *VizieR Online Data Catalog*, 341, 51153
- Seager, S. & Deming, D. 2010, *ARA&A*, 48, 631
- Sestito, P. & Randich, S. 2005, *A&A*, 442, 615
- Steele, I. A., Bates, S. D., Gibson, N., et al. 2008, in *Society of Photo-Optical Instrumentation Engineers (SPIE) Conference Series*, Vol. 7014, *Society of Photo-Optical Instrumentation Engineers (SPIE) Conference Series*
- Torres, G., Andersen, J., & Giménez, A. 2010, *A&A Rev.*, 18, 67
- Triaud, A. e. a. 2010, preprint
- Valenti, J. A. & Fischer, D. A. 2005, *ApJS*, 159, 141
- Valenti, J. A. & Piskunov, N. 1996, *A&AS*, 118, 595